

CONDENSED MATTER PHYSICS

Observation of the quantum valley Hall state in ballistic graphene superlattices

Katsuyoshi Komatsu,^{1*†} Yoshifumi Morita,² Eiichiro Watanabe,³ Daiju Tsuya,³ Kenji Watanabe,⁴ Takashi Taniguchi,⁴ Satoshi Moriyama^{1*}

In graphene superlattices, bulk topological currents can lead to long-range charge-neutral flow and nonlocal resistance near Dirac points. A ballistic version of these phenomena has never been explored. We report transport properties of ballistic graphene superlattices. This allows us to study and exploit giant nonlocal resistances with a large valley Hall angle without a magnetic field. In a low-temperature regime, a crossover occurs toward a new state of matter, referred to as a quantum valley Hall state (qVHS), which is an analog of the quantum Hall state without a magnetic field. Furthermore, a nonlocal resistance plateau, implying rigidity of the qVHS, emerges as a function of magnetic field, and this plateau collapses, which is considered a manifestation of valley/pseudospin magnetism.

INTRODUCTION

The Berry phase (1) is considered an important tool for developing spintronics and valleytronics (2, 3) because it allows control over spin/valley degrees of freedom instead of charge degree of freedom. A particularly challenging problem is engineering the Berry phase through the bulk topological current, which is a descendant the quantum Hall effect (QHE) (4–6) but can occur even in the absence of a magnetic field. Recent discoveries of the quantum anomalous Hall effect (7), which breaks time-reversal symmetry, and quantum spin Hall/topological insulators (8) are also variants of the QHE in terms of topology. Valley current in graphene (9–13) offers promise for realizing the bulk topological current in a (2+1)-dimensional Dirac fermion without a magnetic field (6). Furthermore, valleytronics (2) are expected to fulfill the requirements of the next generation of electronic devices, such as the valley field effect transistor (11, 14).

In monolayer graphene, which exhibits a Dirac-type relativistic energy dispersion (that is, a Dirac cone), one can induce broken inversion symmetry by placing graphene on a hexagonal boron nitride (hBN) substrate with a precise alignment angle near 0°, whereby a long-length moiré pattern appears between the graphene and the hBN lattice because of the 1.8% lattice mismatch between the graphene and the hBN (15–17). The moiré superlattice also induces a fractal energy spectrum under a magnetic field, which is known as Hofstadter's butterfly (15–18). In these systems with broken inversion symmetry, the valley current can be generated and detected via the valley Hall effect (VHE), even in the absence of a magnetic field: The VHE is induced by the accumulated Berry curvature near the apex of the Dirac cone (that is, the hot spot) and is associated with the topological current (9–13). The valley Hall current has not yet been explored near the ballistic regime, and the longitudinal conductivity has always dominated the valley Hall conductivity, implying a small valley Hall angle that veils the nature of the VHE. Observing a coher-

ent neutral long-ranged valley current through an all-electrical method requires nonlocal resistance measurements from a geometry smaller than or comparable to the mean free path (11).

RESULTS AND DISCUSSION

Toward this objective, we fabricated hBN/graphene/hBN heterostructures with one-dimensional Cr/Au contacts, as shown in Fig. 1 (A and B). Sharp increases in the longitudinal resistivity (ρ_{xx}) at backgate voltages V_g of approximately 0 and -21 V correspond to a Dirac point (DP) and a secondary DP (SDP), respectively (Fig. 1C). The emergence of the SDP is a consequence of band modulation due to the moiré superlattice resulting from the alignment of graphene and hBN crystals, indicated by the angle $\theta \sim 0^\circ$, which yields energy gaps at the DP and the SDP. With current and voltage terminals of I : 62, V : 53, Fig. 1C also shows the nonlocal resistance R_{nl} at zero magnetic field. Near the energy bandgap, the hot spots in the graphene due to the hBN, even without a magnetic field, give rise to the transverse bulk topological current, that is, the VHE, which in turn produces a chemical potential difference between terminals 5 and 3, that is, the inverse VHE. We observe a larger R_{nl} of the same order as $h/2e^2$ ($=12.9$ kilohms, where h is the Planck constant and e is the elementary charge) at the SDP. Such a large R_{nl} cannot be explained by the ohmic contribution, assuming diffusive transport with a maximum of 1.5 ohms (see the Supplementary Materials). By contrast, the value of R_{nl} at the DP of approximately 1 kilohm is of the same order as that observed in the previous work (11), and the nonlocal transport at the DP is basically consistent with previous results, implying that bulk valley Hall current emerges and results in nonlocal transport in our device (11). Furthermore, essentially the same phenomena occur at the SDP in the high-temperature regime (see the Supplementary Materials), which implies bulk topological current. However, in the low-temperature regime, the value of R_{nl} at the SDP is even larger than that of ρ_{xx} . In this regime, R_{nl} is within the quantum limit; that is, it equals the quantized value $h/2e^2$ (13) apart from a prefactor of order 1. Furthermore, our results indicate that the R_{nl} itself takes a quantum-limited value and exhibits rigidity under certain conditions, such as a magnetic field, as discussed below. We note that there is an influence of thermal cycles and charge impurities (see the Supplementary Materials). In particular, starting gate voltage fixes the disorder caused by charge impurities. The large disorder effects veil

Copyright © 2018
The Authors, some
rights reserved;
exclusive licensee
American Association
for the Advancement
of Science. No claim to
original U.S. Government
Works. Distributed
under a Creative
Commons Attribution
NonCommercial
License 4.0 (CC BY-NC).

¹International Center for Materials Nanoarchitectonics, National Institute for Materials Science (NIMS), Tsukuba, Ibaraki 305-0044, Japan. ²Faculty of Engineering, Gunma University, Kiryu, Gunma 376-8515, Japan. ³Nanofabrication Platform, NIMS, Tsukuba, Ibaraki 305-0047, Japan. ⁴Research Center for Functional Materials, NIMS, Tsukuba, Ibaraki 305-0044, Japan.

*Corresponding author. Email: katsuyoshi1.komatsu@toshiba.co.jp (K.K.); moriyama.satoshi@nims.go.jp (S.M.)

†Present address: Institute of Memory Technology Research & Development, Toshiba Memory Corporation, Yokkaichi, Mie 512-8550, Japan.

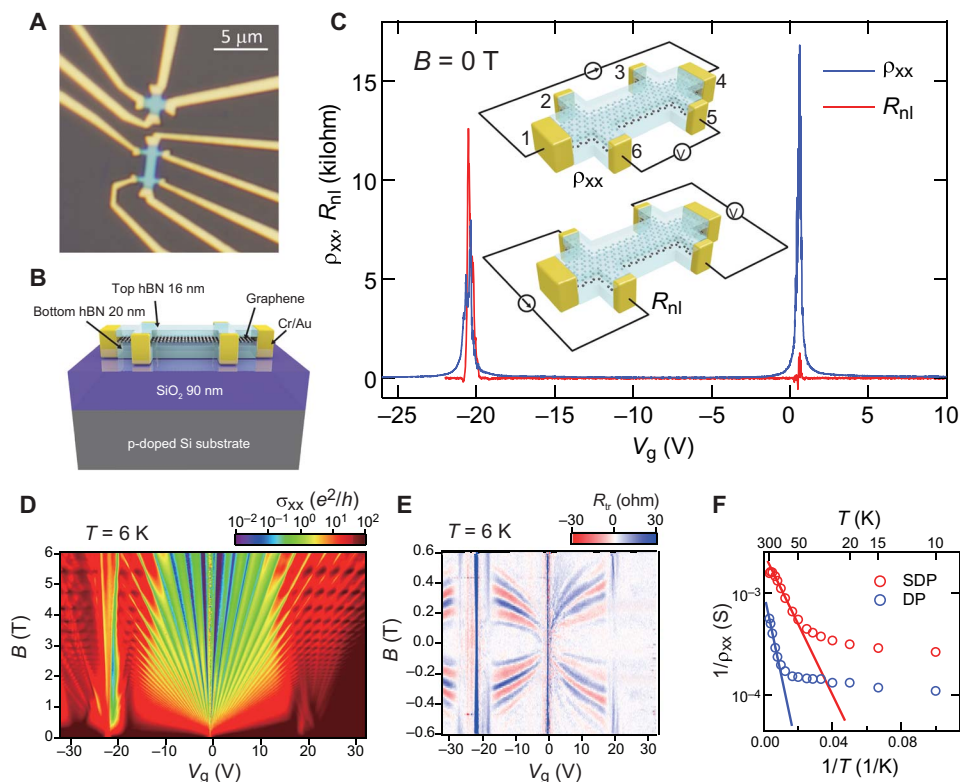


Fig. 1. Device structure and characterization of our hBN/graphene/hBN superlattices. (A) Microscope image of our typical hBN/graphene/hBN superlattice device. The Hall bar geometry is such that width $W = 1.0 \mu\text{m}$ and length $L = 2.5 \mu\text{m}$. (B) Schematic cross section of the device with Cr/Au contacts on the edge yielding one-dimensional contacts. We applied the backgate voltage (V_g) through the 90-nm thickness of SiO_2 and the 20-nm thickness of hBN. (C) (red curve) Measured nonlocal resistance R_{nl} ($I: 62$, $V: 53$) and (blue curve) longitudinal resistivity ρ_{xx} ($I: 14$, $V: 65$) as a function of V_g without magnetic fields at 1.5 K. Sharp increases of the ρ_{xx} at the V_g of approximately 0 and -21 V correspond to a DP and a SDP, respectively. Inset shows schematic pictures of the measurement setup. (D) A logarithmic-scale plot of the longitudinal conductivity (σ_{xx}) as a function of V_g and magnetic fields (B) applied perpendicular to the substrate at 6 K. (E) Transverse resistance (R_{tr}) oscillation at 6 K, which is R_{tr} as a function of V_g and B . The terminal configurations are the same for the R_{nl} in (C). (F) Experimental estimation of the energy gaps derived by the Arrhenius plots of the resistivity of the DP and SDP as a function of measured temperature T . We estimated the gaps to be $E_g = 2\Delta = 32$ and 14 meV at the DP and SDP, respectively.

the giant nonlocal resistance, and that is what happened in previous studies (11).

Figure 1D shows a logarithmic-scale intensity map of the longitudinal conductivity (σ_{xx}) as a function of V_g and a magnetic field B (applied perpendicular to the substrate). We observed the QHE of single-layer graphene near the DP and a Landau-fan diagram of Hofstadter's butterfly. From the periodicity of $1/B$, we estimated the alignment angle between the graphene and hBN, $\theta = 0.7$ to 0.8° , and we estimated the moiré superlattice size to be approximately 11 nm. The mobilities in the sample were up to $250,000 \text{ cm}^2/\text{Vs}$ near the DP and $180,000 \text{ cm}^2/\text{Vs}$ near the SDP at 1.5 K (see the Supplementary Materials). We estimated the mean free path L_f to be 1 to $2 \mu\text{m}$, which is comparable to the sample geometry.

In small magnetic fields, we observed transverse resistance oscillation, as shown in Fig. 1E; we believe this originated from the so-called transverse magnetic focusing (TMF) effect (19). In a ballistic sample, the trajectory of a charged carrier is bent by Lorentz force under a magnetic field, and an injected carrier is focused by the cyclotron motion on the transverse electrode, causing the TMF effect. In our sample, we estimated the distance between the electrodes to be $2.8 \mu\text{m}$, based on $B_f = (2\hbar k_F/eL_{\text{eff}})i = (2\hbar(\pi n)^{1/2}/eL_{\text{eff}})i$, where B_f is the focusing magnetic field, \hbar is the reduced Planck constant given by $h/2\pi$, k_F is the Fermi wave number, L_{eff} is the effective length between electrodes,

n is the carrier density, and i is the number of reflections at the edge; this estimated distance is consistent with the nominal center-to-center length of $2.5 \mu\text{m}$. The TMF is apparent only when the carriers are not scattered while traveling from the injection electrode 6 to the detection electrode 5, thereby achieving the ballistic transport between the electrodes. All of these results confirm the ballistic character of our sample (see the Supplementary Materials).

We estimated the experimental energy gap based on the Arrhenius plots: $1/\rho_{xx} \propto \exp(-E_g/2k_B T)$, where E_g is the gap energy ($=2\Delta$) and k_B is Boltzmann's constant, as shown in Fig. 1F. The gaps were estimated as $E_g = 2\Delta$, being 32 and 14 meV at the DP and SDP, respectively, by linear fitting in the high-temperature region. The gap at the SDP is consistent with that predicted by Moon and Koshino (18), although the gap at the DP is much larger than the predicted value of 2 meV. Woods *et al.* (20) have observed gap openings of approximately 30 meV at the DP in commensurate graphene/hBN superlattices, which is consistent with our results. However, this point remains controversial, and Wang *et al.* (21) have reported recent data from angle-resolved photoemission spectroscopy that support different results. We consider that this point is closely connected to the crossover conditions of the transport picture discussed below. A comment is in order on the different scenarios between the DP and SDP. As discussed below, giant nonlocal resistance occurs only at the SDP in our sample.

A hypothesis is that it is attributable to the larger energy gap in the SDP. However, this point is controversial and contradicts our Arrhenius plots. It is also possible that the gap by the Arrhenius plot is different from the energy gap in the band structure. Because the DP shows a longer mean free path than the SDP, another scenario is that ballistic modes can contribute a negative nonlocal resistance, as discussed by Mayorov *et al.* (22). In contrast to the high-temperature observations, in the lower temperature region, the change of the slope from the Arrhenius form indicates that the carrier transport is dominated by variable range hopping inside the gap due to charge inhomogeneity.

We then investigated the resistances with different terminal configurations in our six-terminal device, and all of the quantum-limited resistance results consistently support the emergence of the quantum valley Hall state (qVHS). In the QHE, we have proposed two different pictures an edge picture and a bulk picture. Although it is unsettled which is valid, it is notable that each gives internally consistent results. In our system, the total Hall conductance, indicated by the topological number (5, 6), vanishes, and there is no a priori reason for edge states to exist. However, recent experimental and theoretical results support the existence of edge states, although their detailed character is determined by their fine electronic structures, which remain to be resolved (23, 24). A mechanism driven by the edge states predicts the giant nonlocal resistance in the quantum limit. Therefore, we calculated the resistances of different configurations using the Landauer-Büttiker formalism with multiterminal samples (25, 26) based on a minimal model in which two edge states for two valleys propagate in opposite directions along the edge, with only nonvanishing elements of the transmission matrix (T) between terminals given by $T_{j+1,j} = T_{j,j+1} = 1$, where j is an integer, which corresponds to the terminal numbers. The current-voltage relationship is given by $I_k = e^2/h \sum_j (T_{jk}V_k - T_{kj}V_j)$, where I_k is the current flowing out of the k -th electrode, V_j is the voltage on the j -th electrode, and T_{jk} is the transmission probability from the j -th to k -th electrode. Solving this equation with an experimental input on I and V , we get I - V relations and resistances. Figure 2 shows the resistances with different terminal configurations of a six-terminal sample. On the basis of the minimal model, we calculated the longitudinal resistance R_{xx} of (I : 14, V : 65) as $h/2e^2$, as shown by the dotted lines in Fig. 2B. We calculated the theoretical R_{nl} of (I : 61, V : 53), (I : 61, V : 54), and (I : 61, V : 43) to be $1/3$, $1/6$, and $1/6$ (unit, h/e^2), respectively, as shown by the dotted lines in Fig. 2C. Similarly, the R_{nl} of (I : 62, V : 53) and (I : 62, V : 43) were $2/3$ and $1/3$ (h/e^2), respectively, as shown by the dotted lines in Fig. 2D. Although the discrepancies between the theoretical predictions may originate from charge impurities (see the Supplementary Materials) and/or the intervalley scattering on the disordered edge with possible dephasing, each R_{nl} is consistent with the theoretical value apart from fluctuation. Furthermore, the spiking behavior of the resistance is reproducible, and we attribute this effect to mesoscopic fluctuation, which can be viewed as a fingerprint of our device and gives an origin of departure from the quantized theoretical values. Their peaks are classified into two values in Fig. 2 (C and D), and the ratio of the two experimental R_{nl} values is close to $1/2$, which implies the existence of channels, as proposed in the minimal edge-state model. Overall, all the longitudinal resistances and resistances with nonlocal geometries show a consistent picture. This is in analogy with the QHE, that is, the qVHS in our device. Although all of the R_{nl} peak shapes were asymmetric and cubic scaling did not fit them at low temperatures, the peak shapes became smooth and fit cubic scaling at higher temperatures (see the Supplementary Materials) (11), part of which is also suggested by recent theoretical simulations (24).

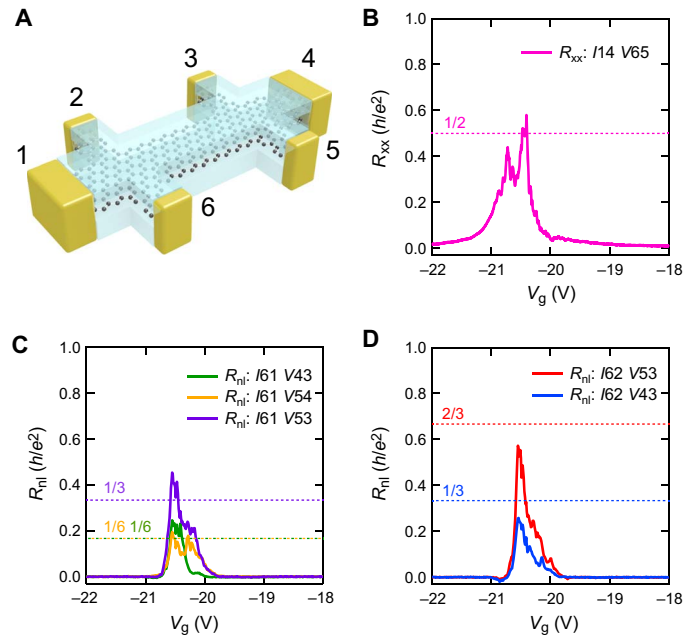


Fig. 2. Longitudinal (local) resistance R_{xx} and nonlocal resistance R_{nl} with different terminal configurations on the six-terminal device measured without magnetic fields at 1.5 K. (A) Schematic showing the terminal number. (B) R_{xx} for (I : 14, V : 65); (C) R_{nl} for (I : 61, V : 53), (I : 61, V : 54), and (I : 61, V : 43); and (D) R_{nl} for (I : 62, V : 43), (I : 62, V : 53), as a function of V_g . Dotted lines show theoretical values of the resistance based on the minimal edge-state model described in the text. Both R_{xx} and R_{nl} are consistent with the theoretical value apart from fluctuations. The ratio of experimental values of R_{nl} (I : 61, V : 53)/ R_{nl} (I : 61, V : 54), R_{nl} (I : 61, V : 53)/ R_{nl} (I : 61, V : 43), and R_{nl} (I : 62, V : 53)/ R_{nl} (I : 62, V : 43) are approximately 2.

Because the qVHS occurs in zero magnetic field with time-reversal symmetry due to the presence of hot spots, its collapse should be connected to the reconstruction of the electronic structure due to a magnetic field through the valley Zeeman energy (VZE), $E_{VZ} = 1/2 g^* \mu_B B$, where g^* is an effective g -factor and μ_B is the Bohr magneton. Koshino and Ando (27) give the theoretical g^* of a single valley as $m^* = \Delta/\nu^2$, $g^* = 2m/m^*$, where m^* is the effective mass, m is the free-electron mass, and ν is the Fermi velocity. In our sample, the g^* was theoretically calculated to be approximately 2500 by using the following parameters: $\Delta = 7$ meV, which is obtained by the Arrhenius plots of the SDP in Fig. 1F, and $\nu = 1.2 \times 10^6$ m/s, which is determined by Shubnikov-de Haas (SdH) oscillations (see the Supplementary Materials). This g^* value of the pseudospin is 1250 times larger than that of a free electron's spin. Figure 3B maps the R_{nl} as a function of V_g and B , showing a robust plateau around the point of zero magnetic field from $B = -0.1$ to $+0.1$ T. This result indicates a rigid qVHS when $2\Delta > 2E_{VZ}$ (Fig. 3A). After the breakdown of the plateau when $2\Delta < 2E_{VZ}$ (Fig. 3A), R_{nl} decreases with increasing magnetic field, approaching zero around 0.8 T (Fig. 3, B and C) and starting to increase in $B > 0.8$ T due to the occurrence of the quantum Hall states (Fig. 3B). The breakdown of the plateau indicates that nonlocal transport is no longer possible because of the breakdown of the hot spots. Actually, the value of VZE at 0.1 T with $g^* = 2500$ is $E_{VZ} = 7$ meV, which agrees with the result for $\Delta = 7$ meV of the SDP. Because the model presented in the study of Koshino and Ando (27) is minimal, a prefactor of order 1 can occur in the valley Zeeman term, which is fixed by the details of the electronic structure at the SDP. In this scenario, in the low-magnetic field regime, we

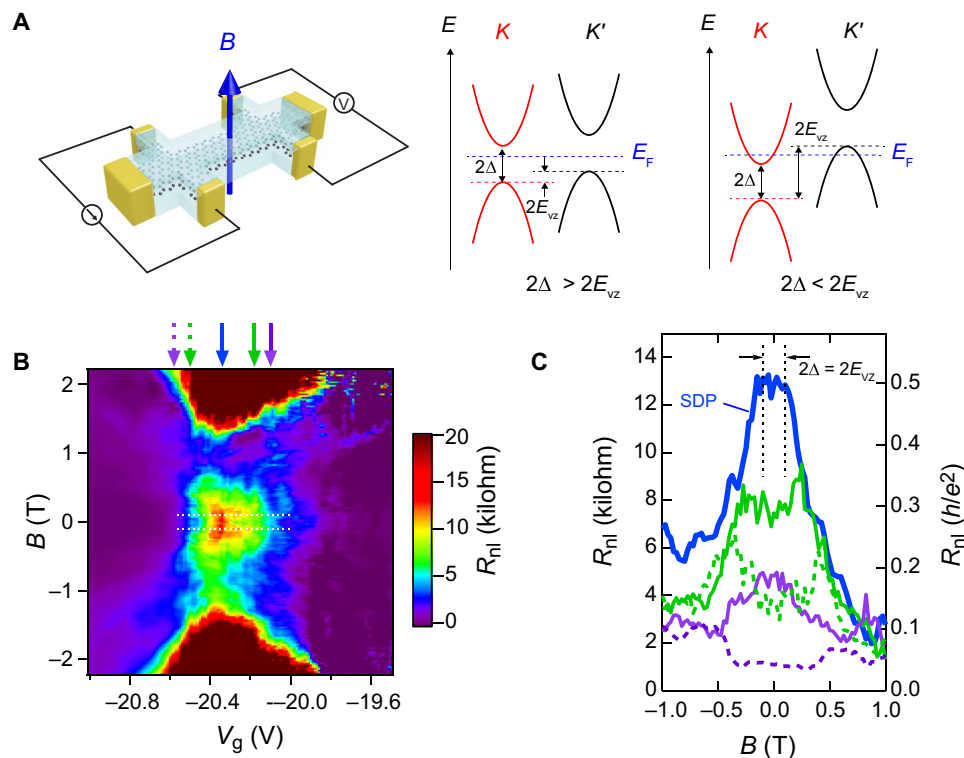


Fig. 3. Nonlocal magnetoresistance in graphene superlattices. (A) Schematics of the measurement setup (left) and the energy band structure in magnetic fields (right), which show how the band structure is reconstructed when the magnetic field is included. In the band structure, we do not take into account the role of orbital magnetism for simplicity, which leads to broadened Landau bands overlapped due to disorder and finite-temperature effects. (B) R_{nl} ($t: 62, V: 53$) is mapped as a function of V_g and B at 1.5 K. Dashed white lines correspond to the plateau denoted by the black arrows in (C). (C) R_{nl} versus B for five V_g 's near the SDP, marked with the same color as arrows on the top of (B). Black arrows show the regime where the energy gap with hot spots is kept, linking to the white dashed lines in (B).

assume that Landau levels are broadened/overlapped because of thermal effects and disorder. Actually, around the collapse of the plateau, we observe no Landau level and cannot detect the SdH signal (see the Supplementary Materials). We observed the clear Landau fan only above near 0.5 T in our sample, as shown in Fig. 1D. This nonlocal magnetoresistance behavior contrasts with the previously reported simple monotonic increase in R_{nl} (11, 28). Our sample, which exhibited lower mobility in several thermal cycles and showed R_{nl} of ~ 1 kilohm, did not show such a clear decrease in the magnetic fields (see the Supplementary Materials), and only samples within the quantum limit with high R_{nl} showed the same behavior. By contrast, R_{nl} in a high-magnetic field regime exhibits a butterfly pattern (see the Supplementary Materials), which should have a QHE origin, and the SdH-type signal does not occur in the low-magnetic field regime (29). As previously reported (28), with a high magnetic field, spin and energy flow should also affect R_{nl} (see the Supplementary Materials).

In summary, we measured nonlocal transport of the ballistic graphene/hBN aligned superlattices with one-dimensional edge contacts. Giant R_{nl} with the order of quantum resistance was observed even at zero magnetic field, indicating the occurrence of the qVHS. Therefore, we conclude that the mechanism driven by the edge states is a more likely scenario for the giant nonlocal resistance in the quantum limit than a bulk-related interpretation. Furthermore, the R_{nl} plateau, which implies a rigidity of the qVHS, emerged as a function of magnetic field, and we also observed its collapse, which we considered a manifestation of valley/pseudospin magnetism. Such an unconven-

tional magnetism should have the potential for engineering the energy-band structure even with a weak magnetic field as well as for spintronics applications.

MATERIALS AND METHODS

Sample fabrication

First, hBN flakes were exfoliated by applying Scotch tape to a poly-methyl methacrylate (PMMA)/polyacrylic acid (PAA)/Si substrate, and then, the substrate was floated on a water surface to isolate the PMMA layer from the Si substrate by dissolving the PAA layer in water. The 16-nm-thick hBN flake was then aligned with a graphene flake exfoliated onto a Si substrate with 90-nm-thick SiO_2 using a homemade atomic layer transfer system (30). The graphene and hBN were carefully aligned along their long edges, and the graphene remained in contact with the hBN flake, forming a graphene/hBN stack. This stack was then aligned with a 20-nm-thick hBN flake that also remained attached to the stack. After removing the PMMA with acetone, we obtained an hBN/graphene/hBN stack on a SiO_2/Si substrate. The sample was annealed at 300°C for 30 min in an Ar/ H_2 atmosphere before atomic force microscopy (AFM) imaging. The AFM image is shown in fig. S1. The Hall bar geometries are indicated by the black lines. We carefully defined the Hall bar geometry so as to include as few bubbles as possible in the channel region, and the sample was then etched into the Hall bar geometry by reactive ion etching using SF_6 . The one-dimensional Cr/Au contacts (31) were deposited by electron beam (EB) evaporation followed by EB lithography with a 125-kV acceleration voltage.

Measurement setup

All of the measurements were performed using both four-terminal dc and low-frequency lock-in techniques (around 17 Hz and ac excitation current of 1 to 10 nA), both of which give consistent results, and measurements were performed in variable temperature cryostats (two types of cryostats were used: base temperatures were 5 and 1.5 K, respectively) with superconducting magnets. All of the experimental data presented in this paper were obtained from the same sample with different cooling cycles from room temperature to below 10 K.

SUPPLEMENTARY MATERIALS

Supplementary material for this article is available at <http://advances.sciencemag.org/cgi/content/full/4/5/eaq0194/DC1>

Supplementary Text

fig. S1. False-color AFM image of our hBN/graphene/hBN stack.

fig. S2. Influence of thermal cycles and charge impurities on our device.

fig. S3. Shubnikov-de Haas oscillation and estimation of the Fermi velocity.

fig. S4. Magnetotransport in our ballistic hBN/graphene/hBN sample.

fig. S5. Temperature dependence of the nonlocal resistance R_{nl} .

fig. S6. Magnetic field dependence of the R_{nl} .

References (32–42)

REFERENCES AND NOTES

- M. V. Berry, Quantal phase factors accompanying adiabatic changes. *Proc. R. Soc. A* **392**, 45–57 (1984).
- A. Rycerz, J. Tworzydło, C. W. J. Beenakker, Valley filter and valley valve in graphene. *Nat. Phys.* **3**, 172–175 (2007).
- A. Cresti, B. K. Nikolić, J. H. García, S. Roche, Charge, spin and valley Hall effects in disordered graphene. *Riv. Nuovo Cimento* **39**, 587 (2016).
- R. B. Laughlin, Quantized Hall conductivity in two dimensions. *Phys. Rev. B* **23**, 5632–5633 (1981).
- D. J. Thouless, M. Kohmoto, M. P. Nightingale, M. den Nijs, Quantized Hall conductance in a two-dimensional periodic potential. *Phys. Rev. Lett.* **49**, 405–408 (1982).
- F. D. M. Haldane, Model for a quantum Hall effect without Landau levels: Condensed-matter realization of the “parity anomaly”. *Phys. Rev. Lett.* **61**, 2015–2018 (1988).
- C.-Z. Chang, J. Zhang, X. Feng, J. Shen, Z. Zhang, M. Guo, K. Li, Y. Ou, P. Wei, L.-L. Wang, Z.-Q. Ji, Y. Feng, S. Ji, X. Chen, J. Xia, X. Dai, Z. Fang, S.-C. Zhang, K. He, Y. Wang, L. Lu, X.-C. Ma, Q.-K. Xue, Experimental observation of the quantum anomalous Hall effect in a magnetic topological insulator. *Science* **340**, 167–170 (2013).
- A. Roth, C. Brüne, H. Buhmann, L. W. Molenkamp, J. Maciejko, X.-L. Qi, S.-C. Zhang, Nonlocal transport in the quantum spin Hall state. *Science* **325**, 294–297 (2009).
- D. Xiao, W. Yao, Q. Niu, Valley-contrasting physics in graphene: Magnetic moment and topological transport. *Phys. Rev. Lett.* **99**, 236809 (2007).
- D. Xiao, M.-C. Chang, Q. Niu, Berry phase effects on electronic properties. *Rev. Mod. Phys.* **82**, 1959–2007 (2010).
- R. V. Gorbachev, J. C. W. Song, G. L. Yu, A. V. Kretinin, F. Withers, Y. Cao, A. Mishchenko, I. V. Grigorieva, K. S. Novoselov, L. S. Levitov, A. K. Geim, Detecting topological currents in graphene superlattices. *Science* **346**, 448–451 (2014).
- Y. D. Lensky, J. C. W. Song, P. Samutpraphoot, L. S. Levitov, Topological valley currents in gapped Dirac materials. *Phys. Rev. Lett.* **114**, 256601 (2015).
- T. Ando, Theory of valley Hall conductivity in graphene with gap. *J. Phys. Soc. Jpn.* **84**, 114705 (2015).
- M.-K. Lee, N.-Y. Lue, C.-K. Wen, G. Y. Wu, Valley-based field-effect transistors in graphene. *Phys. Rev. B* **86**, 165411 (2012).
- L. A. Ponomarenko, R. V. Gorbachev, G. L. Yu, D. C. Elias, R. Jalil, A. A. Patel, A. Mishchenko, A. S. Mayorov, C. R. Woods, J. R. Wallbank, M. Mucha-Kruczynski, B. A. Piot, M. Potemski, I. V. Grigorieva, K. S. Novoselov, F. Guinea, V. I. Fal'ko, A. K. Geim, Cloning of Dirac fermions in graphene superlattices. *Nature* **497**, 594–597 (2013).
- C. R. Dean, L. Wang, P. Maher, C. Forsythe, F. Ghahari, Y. Gao, J. Katoch, M. Ishigami, P. Moon, M. Koshino, T. Taniguchi, K. Watanabe, K. L. Shepard, J. Hone, P. Kim, Hofstadter's butterfly and the fractal quantum Hall effect in moiré superlattices. *Nature* **497**, 598–602 (2013).
- B. Hunt, J. D. Sanchez-Yamagishi, A. F. Young, M. Yankowitz, B. J. LeRoy, K. Watanabe, T. Taniguchi, P. Moon, M. Koshino, P. Jarillo-Herrero, R. C. Ashoori, Massive Dirac fermions and Hofstadter butterfly in a van der Waals heterostructure. *Science* **340**, 1427–1430 (2013).
- P. Moon, M. Koshino, Electronic properties of graphene/hexagonal-boron-nitride moiré superlattice. *Phys. Rev. B* **90**, 155406 (2014).
- T. Taychatanapat, K. Watanabe, T. Taniguchi, P. Jarillo-Herrero, Electrically tunable transverse magnetic focusing in graphene. *Nat. Phys.* **9**, 225–229 (2013).
- C. R. Woods, L. Britnell, A. Eckmann, R. S. Ma, J. C. Lu, H. M. Guo, X. Lin, G. L. Yu, Y. Cao, R. V. Gorbachev, A. V. Kretinin, J. Park, L. A. Ponomarenko, M. I. Katsnelson, Y. N. Gornostyrev, K. Watanabe, T. Taniguchi, C. Casiraghi, H.-J. Gao, A. K. Geim, K. S. Novoselov, Commensurate-incommensurate transition in graphene on hexagonal boron nitride. *Nat. Phys.* **10**, 451–456 (2014).
- E. Wang, X. Lu, S. Ding, W. Yao, M. Yan, G. Wan, K. Deng, S. Wang, G. Chen, L. Ma, J. Jung, A. V. Fedorov, Y. Zhang, G. Zhang, S. Zhou, Gaps induced by inversion symmetry breaking and second-generation Dirac cones in graphene/hexagonal boron nitride. *Nat. Phys.* **12**, 1111–1115 (2016).
- A. S. Mayorov, R. V. Gorbachev, S. V. Morozov, L. Britnell, R. Jalil, L. A. Ponomarenko, P. Blake, K. S. Novoselov, K. Watanabe, T. Taniguchi, A. K. Geim, Micrometer-scale ballistic transport in encapsulated graphene at room temperature. *Nano Lett.* **11**, 2396–2399 (2011).
- M. J. Zhu, A. V. Kretinin, M. D. Thompson, D. A. Bandurin, S. Hu, G. L. Yu, J. Birkbeck, A. Mishchenko, I. J. Vera-Marun, K. Watanabe, T. Taniguchi, M. Polini, J. R. Prance, K. S. Novoselov, A. K. Geim, M. Ben Shalom, Edge currents shunt the insulating bulk in gapped graphene. *Nat. Commun.* **8**, 14552 (2017).
- J. M. Marmolejo-Tejada, J. H. García, P.-H. Chang, X.-L. Sheng, A. Cresti, S. Roche, B. K. Nikolić, Origin of nonlocal resistance in multiterminal graphene on hexagonal-boron nitride: Fermi surface edge states or Fermi sea topological valley currents. arXiv: condmat/1706.09361v1 (2017).
- R. Landauer, Spatial variation of currents and fields due to localized scatterers in metallic conduction. *IBM J. Res. Dev.* **1**, 223–231 (1957).
- M. Büttiker, Absence of backscattering in the quantum Hall effect in multiprobe conductors. *Phys. Rev. B* **38**, 9375–9389 (1988).
- M. Koshino, T. Ando, Anomalous orbital magnetism in Dirac-electron systems: Role of pseudospin paramagnetism. *Phys. Rev. B* **81**, 195431 (2010).
- D. A. Abanin, S. V. Morozov, L. A. Ponomarenko, R. V. Gorbachev, A. S. Mayorov, M. I. Katsnelson, K. Watanabe, T. Taniguchi, K. S. Novoselov, L. S. Levitov, A. K. Geim, Giant nonlocality near the Dirac point in graphene. *Science* **332**, 328–330 (2011).
- V. Y. Tsaran, S. G. Sharapov, Magnetic oscillations of the anomalous Hall conductivity. *Phys. Rev. B* **93**, 075430 (2016).
- C. R. Dean, A. F. Young, I. Meric, C. Lee, L. Wang, S. Sorgenfrei, K. Watanabe, T. Taniguchi, P. Kim, K. L. Shepard, J. Hone, Boron nitride substrates for high-quality graphene electronics. *Nat. Nanotechnol.* **5**, 722–726 (2010).
- L. Wang, I. Meric, P. Y. Huang, Q. Gao, Y. Gao, H. Tran, T. Taniguchi, K. Watanabe, L. M. Campos, D. A. Muller, J. Guo, P. Kim, J. Hone, K. L. Shepard, C. R. Dean, One-dimensional electrical contact to a two-dimensional material. *Science* **342**, 614–617 (2013).
- A. H. Castro Neto, F. Guinea, N. M. R. Peres, K. S. Novoselov, A. K. Geim, The electronic properties of graphene. *Rev. Mod. Phys.* **81**, 109–162 (2009).
- D. C. Elias, R. V. Gorbachev, A. S. Mayorov, S. V. Morozov, A. A. Zhukov, P. Blake, L. A. Ponomarenko, I. V. Grigorieva, K. S. Novoselov, F. Guinea, A. K. Geim, Dirac cones reshaped by interaction effects in suspended graphene. *Nat. Phys.* **7**, 701–704 (2011).
- C. W. J. Beenakker, H. van Houten, Quantum transport in semiconductor nanostructures. *Solid State Phys.* **44**, 1–228 (1991).
- S. Masubuchi, K. Iguchi, T. Yamaguchi, M. Onuki, M. Arai, K. Watanabe, T. Taniguchi, T. Machida, Boundary scattering in ballistic graphene. *Phys. Rev. Lett.* **109**, 036601 (2012).
- D. A. Abanin, A. V. Shytov, L. S. Levitov, B. I. Halperin, Nonlocal charge transport mediated by spin diffusion in the spin Hall effect regime. *Phys. Rev. B* **79**, 035304 (2009).
- M. Beconcini, F. Taddei, M. Polini, Nonlocal topological valley transport at large valley Hall angles. *Phys. Rev. B* **94**, 121408 (R) (2016).
- M. Sui, G. Chen, L. Ma, W.-Y. Shan, D. Tian, K. Watanabe, T. Taniguchi, X. Jin, W. Yao, D. Xiao, Y. Zhang, Gate-tunable topological valley transport in bilayer graphene. *Nat. Phys.* **11**, 1027–1031 (2015).
- Y. Shimazaki, M. Yamamoto, I. V. Borzenets, K. Watanabe, T. Taniguchi, S. Tarucha, Generation and detection of pure valley current by electrically induced Berry curvature in bilayer graphene. *Nat. Phys.* **11**, 1032–1036 (2015).
- M. Yamamoto, Y. Shimazaki, I. V. Borzenets, S. Tarucha, Valley Hall effect in two-dimensional hexagonal lattices. *J. Phys. Soc. Jpn.* **84**, 121006 (2015).
- L. J. van der Pauw, A method of measuring the resistivity and Hall coefficient on lamellae of arbitrary shape. *Philips Tech. Rev.* **20**, 220–224 (1958).
- J. Renard, M. Studer, J. A. Folk, Origins of nonlocality near the neutrality point in graphene. *Phys. Rev. Lett.* **112**, 116601 (2014).

Acknowledgments: We thank H. Osato of National Institute for Materials Science (NIMS) for technical support of the fabrication process, K. Wakabayashi of Kwansai Gakuin University, M. Koshino of Osaka University, B. K. Nikolić of the University of Delaware, S. Sharapov of the Bogolyubov Institute for Theoretical Physics, and S. Nakaharai of NIMS for useful comments

and discussions. **Funding:** The device fabrication and measurement were supported by the Japan Society for Promotion of Science (JSPS) KAKENHI 15K18058, 26630139, and 25706030; and the NIMS Nanofabrication Platform Project, the World Premier International Research Center Initiative on Materials Nanoarchitectonics, sponsored by the Ministry of Education, Culture, Sports, Science and Technology (MEXT), Japan. Growth of hBN was supported by the Elemental Strategy Initiative conducted by the MEXT, Japan and JSPS KAKENHI 15K21722. **Author contributions:** K.K. and S.M. conceived and designed the experiments. K.K., E.W., and D.T. fabricated the devices. K.K. and S.M. performed the experiments. K.K., Y.M., and S.M. analyzed the data, developed the models, and wrote the paper. K.W. and T.T. provided the hBN crystals used in the devices. **Competing interests:** The authors declare that they have no competing interests. **Data and materials availability:** All data needed to evaluate the

conclusions in the paper are present in the paper and/or the Supplementary Materials. Additional data related to this paper may be requested from the authors.

Submitted 21 September 2017

Accepted 4 April 2018

Published 18 May 2018

10.1126/sciadv.aag0194

Citation: K. Komatsu, Y. Morita, E. Watanabe, D. Tsuya, K. Watanabe, T. Taniguchi, S. Moriyama, Observation of the quantum valley Hall state in ballistic graphene superlattices. *Sci. Adv.* **4**, eaaq0194 (2018).